ACS OMEGA

Open Access

http://pubs.acs.org/journal/acsodf

Article

Propane Dehydrogenation Catalyzed by Pt Clusters (Pt_2−Pt_6) in Gas Phase and Supported on g-C_3N_4 and γ-Al_2O_3: A Theoretical Study

Jie Pan, Gerard Bru, Jorge J. Carbó, Cyril Godard, and Josep M. Ricart*

Cite This: *ACS Omega* 2025, 10, 46105−46114

Read Online

ACCESS | Metrics & More | Article Recommendations | Supporting Information

ABSTRACT: Density functional theory (DFT) investigations and microkinetic analyses were conducted to explore the propane dehydrogenation (PDH) process catalyzed by small platinum clusters (Pt_2−Pt_6). γ-Al_2O_3 and graphitic carbon nitride (g-C_3N_4) were considered as support materials to evaluate their influence on the catalytic performance. Among the studied clusters, Pt_5 demonstrated superior PDH activity, selectivity, and stability. Notably, the presence of supports significantly enhanced the selectivity of the reaction, with the Pt_5/g-C_3N_4 system exhibiting the most favorable performance.

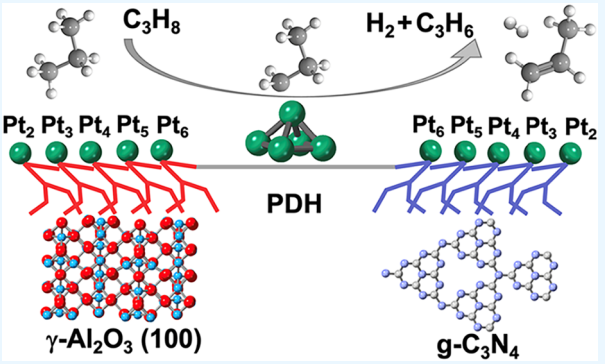

INTRODUCTION

The production of light olefins, including ethylene, propylene, and butene, is highly important to the global chemical industry and plays a critical role in the production of a vast array of everyday products. Driven by sustained economic growth, a rising global population, and expanding industrial output, the demand for these critical feedstocks continues to increase. Among them, propylene stands out due to its exceptional versatility and wide range of applications. It serves as a key precursor for the manufacture of numerous high-value chemicals and materials, such as polypropylene, acetone, acrylonitrile, acrolein, acrylic acid, acrylates, and propylene oxide. As a result of this surging demand, an increasingly pronounced supply-demand gap has emerged, emphasizing the need for efficient and sustainable production routes for propylene.[1,2]

In response, various methodologies have been developed for propylene production, such as the methanol-to-olefins, the Fischer−Tropsch-to-olefins process, and the propane dehydrogenation (PDH).[3−9] Among these, PDH is especially promising owing to its straightforward feed−product relationship and economical use of propane.[1,10] Furthermore, hydrogen, generated as a valuable byproduct, increases the interest in this process. Industrial implementation typically requires high temperatures (550−750 °C) and low partial pressures (∼0.1 MPa) due to the highly endothermic nature of the reaction (ΔH^0 = 123.8 kJ mol^{-1} at 298.15 K), so robust and highly active catalysts are needed to efficiently cleave the C−H bonds of propane.[11]

Conventionally, platinum- and chromium-based catalysts have been employed for PDH.[1,12,13] Chromium oxides, while cost-effective, pose environmental and health hazards and suffer rapid deactivation via side reactions.[1] In contrast, platinum-based systems offer superior environmental compatibility and greater resistance to deactivation, although they are still susceptible to side reactions such as deep dehydrogenation and coke formation.[12−14] Enhancing their performance requires fine-tuning both activity and selectivity, which can be addressed by controlling catalyst morphology and support interactions.[14−16]

Cluster size is a critical factor that influences catalytic behavior. Experimentally, Zhu and Chen et al.[17] have shown that small Pt clusters dominated by low-coordination metal atoms exhibit enhanced C−H bond activation, while larger clusters with Pt(111) facets favor weaker binding of propene, improving selectivity. Computed catalytic activities of various Pt_n clusters (n = 2−6) reveal different C−H activation energies (E_a) for the first bond breaking of propane, indicating the effect of cluster size on catalytic activity.[18] However, this study lacked an analysis of key factors such as the second C−H bond cleavage and product desorption energies. Therefore, it is pertinent to investigate these aspects.

Another essential strategy involves tailoring the interaction between the metal clusters and suitable supports. Metal−support interactions not only influence cluster dispersion and

Received: July 31, 2025
Revised: September 6, 2025
Accepted: September 15, 2025
Published: September 25, 2025

stability but also can modulate electronic properties to improve catalytic performance. In an experimental study, Vajda and Curtiss et al.[19] deposited size preselected Pt_{8-10} clusters on porous aluminum oxide and reported a 40-fold increase in activity compared with the conventional catalyst for the oxidative dehydrogenation of propane, while maintaining high selectivity to propene. They also use DFT to study PDH on a Pt_4 cluster and attribute the high activity to the low coordination of Pt within the clusters, favoring the C−H bond breaking over that of C−C or C═C bonds.[19]

Supported clusters have consequently attracted significant attention as effective catalysts for PDH. In particular, γ-Al_2O_3 is considered one of the most versatile oxide supports due to its remarkable porosity.[20−22] Moreover, Al^{3+} penta-coordinated sites (Al_p) on the (100) facets of γ-Al_2O_3 are favorable anchoring points for Pt clusters, mitigating sintering and improving durability.[23] Therefore, the γ-Al_2O_3(100) surface is selected as a reference for anchoring Pt_n, compared with the naked Pt_n subnanometric clusters, and further investigates the impact of oxide supports on Pt_n clusters' properties toward PDH.

Additionally, supports like graphene, doped graphene, or graphitic carbon nitride (g-C_3N_4) have emerged as promising nonoxide alternatives. Thus, it is pertinent to compare with nonoxide supports such as graphene. However, pristine graphene is not suitable as a support under high-temperature reaction conditions due to the tendency of metal clusters to diffuse and aggregate on its surface.[24] Consequently, research efforts have turned toward modifying graphene through the introduction of vacancies and heteroatoms, a strategy that effectively incorporates g-C_3N_4, which combines both structural features. The morphology of g-C_3N_4 resembles fragments of graphene interconnected by tertiary amines, accompanied by uniformly distributed holes and abundant lone pairs of electrons originating from nitrogen atoms.[24−27]

Within our previous computational studies on PDH by Pt catalysts, reactive ReaxFF simulations found that in the stepped Pt(211) facet, propane activation occurs in low coordinated Pt atoms at the step, resulting in a more reactive and selective surface topology than Pt(111) and Pt(100) ones.[28] Thus, we expect that small clusters with low coordinated morphologies would lead to highly active and selective catalysts. Indeed, we performed DFT calculations and ab initio molecular dynamics (AIMD) simulations on the Pt_1 atom and the Pt_4 clusters supported on g-C_3N_4. However, both systems showed some limitations in PDH catalysis. In the single-atom (Pt_1/g-C_3N_4) system, the Pt atom can diffuse below the surface of the support, while in the single-cluster (Pt_4/g-C_3N_4) one, deep dehydrogenated species cover the active sites, lowering the activity.[29]

In this study, we advance the understanding of factors that optimize propane dehydrogenation in platinum-based catalysts by examining the influence of cluster size and support material. Specifically, we perform a theoretical study of small platinum clusters (Pt_2 to Pt_6), both naked and supported on γ-Al_2O_3 and g-C_3N_4, evaluating how these variables influence catalytic performance.

COMPUTATIONAL DETAILS

All calculations were performed using the Vienna Ab Initio Simulation Package (VASP 5.3.5), with the same settings as in our previous work.[29,30] Projector augmented wave (PAW) pseudopotentials were used to describe the core electron density and its interaction with the valence electron density.[31] The exchange−correlation interactions were calculated using the PBE-generalized gradient approximation (GGA) functional.[32] The van der Waals interactions were considered by the DFT-D3 method with zero-damping of Grimme.[33] Spin polarization and dipole correction were always included. The residual force and energy convergence criteria were set to 1×10^{-3} eV/Å and 1×10^{-5} eV, respectively. A plain wave energy cutoff of 400 eV for the valence electron expansion was selected, and a Monkhorst−Pack mesh with a $2 \times 2 \times 1$ k-point grid was used to sample the Brillouin zone, in accordance with previous papers on Pt_n/γ-Al_2O_3(100) and further tested for g-C_3N_4.[23,29] A $2 \times 2 \times 1$ supercell ($14.246 \times 14.250 \times 22$ Å^3 for g-C_3N_4 and $16.826 \times 11.174 \times 28$ Å^3 for γ-Al_2O_3) was used to avoid unwanted interactions between repeated slabs. A cube of $15 \times 15 \times 15$ Å^3 with a k-point grid of $1 \times 1 \times 1$ was used for isolated Pt atoms and naked clusters (Pt_n). The transition states (TS) of elementary reactions were obtained by the dimer method with the input files referring to a previous study.[29] The proper character of the local minima and the TS has been confirmed by vibrational frequencies analysis, ensuring a single imaginary frequency for every TS, and the absence of imaginary frequencies for reactants, intermediates, and products.

In addition, Bader's atoms-in-molecules electronic density analysis[34] was also carried out to obtain atomic charges via integration of electronic density within regions delimited by zero flux surfaces, allowing for the evaluation of the charge transfer between species.

The cohesive energies (E_{coh}) of Pt particles were calculated as follows:

$$E_{coh} = (E_{Pt_n} - nE_{Pt})/n \quad (1)$$

where n is the number of Pt atoms, E_{Pt_n} stands for the energy of Pt_n; E_{Pt} is the energy of gas phase Pt in its ground state.

The interaction energy (E_{int}) of Pt with the surfaces was calculated by

$$E_{int} = (E_{Pt@support} - E_{support} - nE_{Pt})/n \quad (2)$$

where $E_{Pt@support}$ is the energy of the anchored metal on the support. $E_{support}$ is the energy of the support.

The adsorption energy for each adsorbed species is calculated by eq 3.

$$E_{ads} = E_{mol\text{-}Pt@support} - (E_{mol} + E_{Pt@support}) \quad (3)$$

where $E_{mol\text{-}Pt@support}$ is the energy of the whole system; E_{mol} stands for the energy of the adsorbed molecule in the gas phase; and $E_{Pt@support}$ is the energy of the catalyst. The energy profiles were made with reference to propane in the gas phase and the clean surface. Besides the thermodynamic treatment, the microkinetic modeling (MKM) was also used to study the kinetic properties of the catalysts, and both details are in the Supporting Information.

RESULTS AND DISCUSSION

Structure of Pt_n Clusters (n = 2−6). First, we optimized the bare clusters, taking into account both 2D and 3D configurations (Figure 1). Note that the 2D configurations appear to be the most stable, as described by Da Silva et al.[35] As shown in Figure 1, the Pt−Pt bond distances range from 2.330 Å to 2.613 Å, consistent with previous theoretical and experimental findings.[36,37] For clusters with the same number

https://doi.org/10.1021/acsomega.5c07626
ACS Omega 2025, 10, 46105−46114

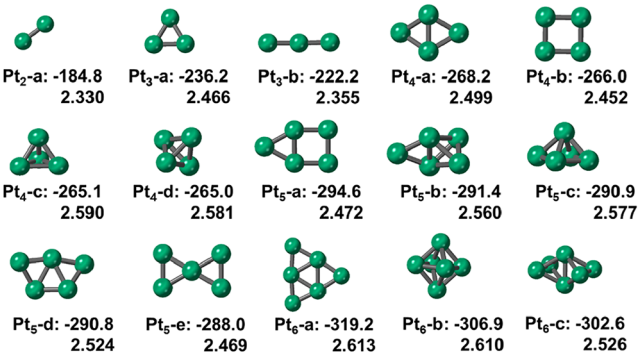

Figure 1. Side views of the bare Pt_n clusters (n = 2−6). The cohesive energies (E_{coh}) in kJ/mol (top) and average Pt−Pt bond distances in Å (bottom) are indicated.

of Pt atoms, the cohesive energies (E_{coh}, Figure S1) are similar, but 2D configurations are slightly more stable than 3D ones, with the difference being larger for Pt_6.[35,38] Our results are also in agreement with previous reports,[35] which described that planar configurations were more stable for small Pt clusters, while 3D configurations became more favorable for clusters larger than Pt_{10}. The E_{coh} increases with the cluster size and gradually converges to the bulk value (−511 kJ/mol), see Figure S1.[39]

Pt_n (n = 2−6) Clusters Supported on γ-Al_2O_3. Next, γ-Al_2O_3-supported Pt_n clusters were examined. Previous studies demonstrated that Al^{3+} sites (Al_p) residing on (100) facets exhibit the highest affinity for capturing Pt atoms, so the γ-Al_2O_3(100) surface was selected (Figure 2a).[23,40]

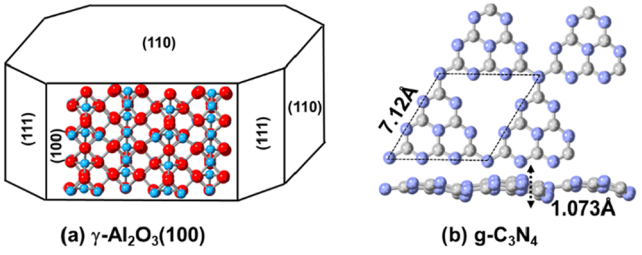

Figure 2. (a) Top view of γ-Al_2O_3(100) and (b) top and side views of g-C_3N_4. Al, O, C, and N are in blue, red, gray, and lavender, respectively.

The dehydrated γ-Al_2O_3(100) facet was used as described in the model proposed by Digne and Sautet et al.[41,42] When the adsorption of the Pt_n clusters on γ-Al_2O_3(100) (Figure 3) was examined, distortion on the surface was observed due to the electronic exchange between the support and clusters, which was previously documented.[43,44] The interaction energies (E_{int}) initially decreased with increasing cluster size, but the differences gradually diminished, and for Pt_5 and Pt_6, the difference became negligible. Additionally, for some configurations, the most favorable ones were not those corresponding to the adsorption of planar clusters, such as the structure of AL-**Pt_4-d**. This can be attributed to the fact that the morphology of the supported clusters is controlled by the competition of the metal−surface and metal−metal interactions.[36] By further comparison of the E_{coh} (which evaluates the aggregation capacity of the clusters, Figure 1) and E_{int} (which evaluates the binding energy between the cluster and the support, Figure 3), we observe that the E_{int} values are consistently more negative than the E_{coh}, meaning that the clusters interact strongly with alumina and are less prone to sinter. Furthermore, the difference between E_{int} and E_{coh} slowly decreases with increasing cluster size.

Pt_n (n = 2−6) Clusters Supported on g-C_3N_4. Next, we analyze the structures and interaction energies of Pt clusters supported on g-C_3N_4, whose structure and lattice were taken from our previous study,[29] see Figure 2b. The configurations of all of the Pt_n clusters adsorbed on g-C_3N_4 are given in Figure 4. The results were similar to those of Pt_n/γ-Al_2O_3(100). The most stable adsorbed configuration is not always planar, as observed in the case of Pt_5 clusters, where the **Pt_5-c** structure shows the largest interaction energy. The cluster−support interaction becomes stronger as cluster size increases until it reaches the maximum strength for Pt_5. The E_{int} is always greater (in absolute value) than the cluster E_{coh}.

Comparing the results for the two supports (Figures 3 and 4), we observe qualitatively similar interaction energies, which, depending on cluster size, are larger for the γ-Al_2O_3(100) or the g-C_3N_4 supports. For each cluster composition (Pt_{2-6}), the structure with the largest calculated interaction energy is labeled as **Pt_n-a**, but we did not identify any obvious tendency or the same type of cluster for both types of support. Therefore, for the sake of simplicity (also due to their similar E_{int} and E_{coh} along the series of studied clusters compared to the most stable ones), we selected the following regular Pt_n clusters: linear ones for Pt_2 (**Pt_2-a**, **AL-Pt_2-a**, **CN-Pt_2-a**), triangular ones for Pt_3 cluster (**Pt_3-a**, **AL-Pt_3-a**, **CN-Pt_3-a**), pyramid ones for Pt_4 (**Pt_4-c**, **AL-Pt_4-b**, **CN-Pt_4-c**), square pyramid ones for Pt_5 (**Pt_5-c**, **AL-Pt_5-b**, **CN-Pt_5-a**), and octahedral ones for Pt_6 (**Pt_6-b**, **AL-Pt_6-b**, **CN-Pt_6-b**) were selected to study the catalytic performance for PDH.

Catalytic Performance of Bare and Supported Pt_n Clusters (n = 2−6) in PDH. The stability of catalysts is one of the main factors to evaluate the performance of heterogeneous catalysts, which is expressed as the balance between E_{coh} and E_{int}.[39] Although it has been briefly discussed above, a further comparison is made in Figure 5a. We can see that E_{coh} is always weaker than E_{int} on both supports, indicating that adsorption is more favorable than cluster aggregation for all the clusters and that the E_{coh} decreases as the cluster size increases, converging toward the bulk value.[39] For Pt_n/γ-Al_2O_3(100), the surface−cluster interaction strengthens as cluster size increases. Moreover, the downward trend gradually weakens, resulting in only a 4.9 kJ/mol difference between Pt_5 and Pt_6; for Pt_n/g-C_3N_4, similar results are detected for Pt_2 to Pt_5, but for Pt_6, the E_{int} is stronger by 28.8 kJ/mol compared with Pt_5, since only a maximum of 4 Pt atoms can interact with N atoms due to the size of the g-C_3N_4 hole. Finally, for Pt_2 to Pt_5, the adsorption energy on g-C_3N_4 is stronger than on γ-Al_2O_3(100), while for Pt_6, it is the opposite, due to the change in E_{int} of Pt_6 on g-C_3N_4.

The atomic charge was analyzed using the Bader approach, as shown in Figure 5b. As a reference, the Bader charges of bulk α-PtO_2 were calculated. The computed charge on the Pt atoms was 1.4 |e|, close to the value recently reported by Wang et al. of 1.6 |e|.[45] The atomic charges of Pt atoms in the bare neutral clusters are, as expected, close to zero. The charges of γ-Al_2O_3(100)-supported clusters are slightly negative, in agreement with the results reported by Sautet et al.[39] The charges of the supported clusters on g-C_3N_4 are slightly positive, similar to the case of metal species anchored on N-doped carbon materials.[46,47] However, as the size of clusters

https://doi.org/10.1021/acsomega.5c07626
ACS Omega 2025, 10, 46105−46114

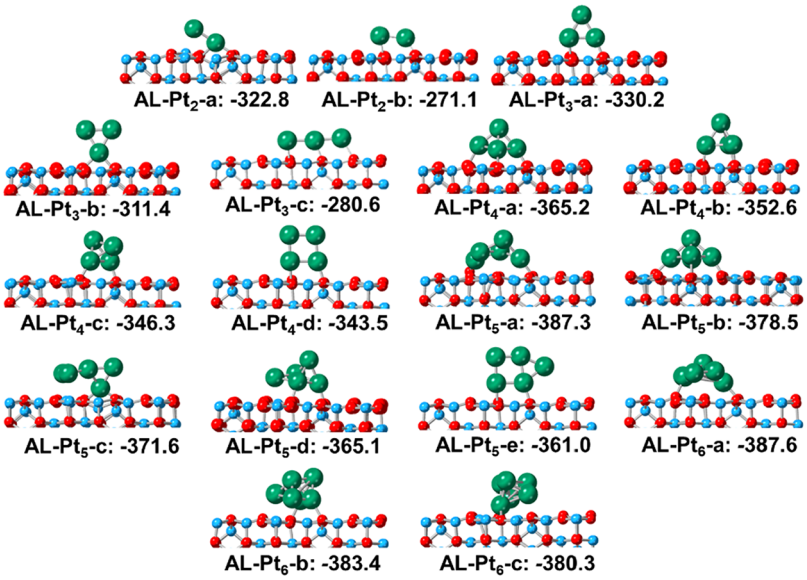

Figure 3. Side views of $Pt_n/\gamma\text{-}Al_2O_3(100)$. Al, O, and Pt atoms are in blue, red, and green, respectively. The interaction energies (E_{int}, kJ/mol) between clusters and the surface are indicated. AL stands for the alumina support.

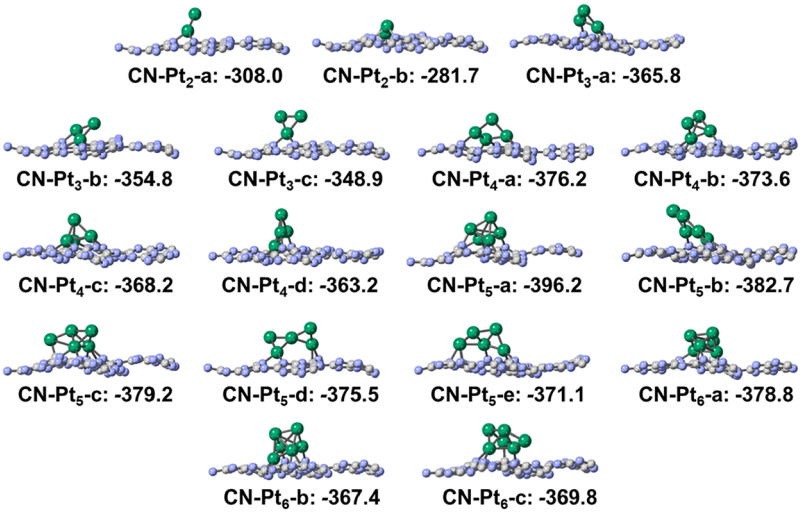

Figure 4. Side views of $Pt_n/g\text{-}C_3N_4$. C, N, and Pt atoms are in gray, lavender, and green, respectively. The interaction energies (E_{int}, kJ/mol) are indicated. CN stands for carbon nitride support.

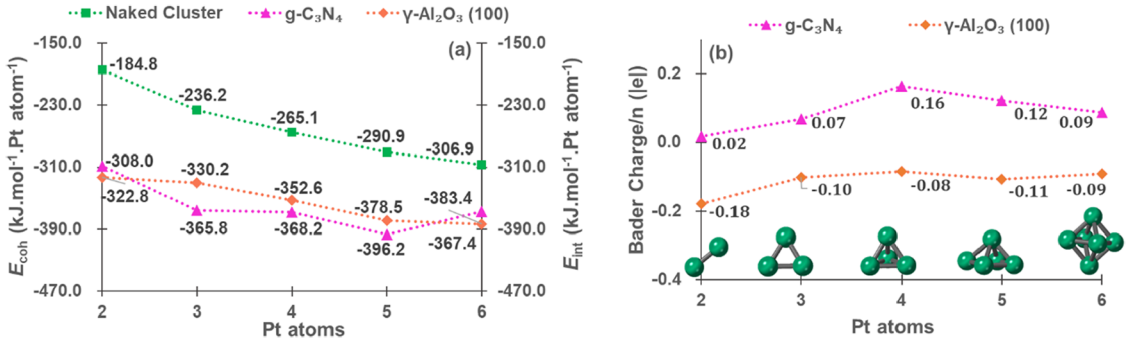

Figure 5. (a) E_{coh} of bare Pt_n clusters and E_{int} between Pt_n and $\gamma\text{-}Al_2O_3(100)$ or $g\text{-}C_3N_4$, all energies in kJ/mol. (b) Bader charge of naked and supported Pt_n clusters (mean charge per Pt atom) as a function of cluster size, the charge for each Pt atom is shown in Table S1.

increases, the charge transfer between clusters and both supports decreases, setting atomic charges close to zero.

As the initial step of PDH, we computed the adsorption of propane on all of the catalysts. Adsorption through either primary carbon (C_1) or secondary (C_2) led to similar results

https://doi.org/10.1021/acsomega.5c07626
ACS Omega 2025, 10, 46105−46114

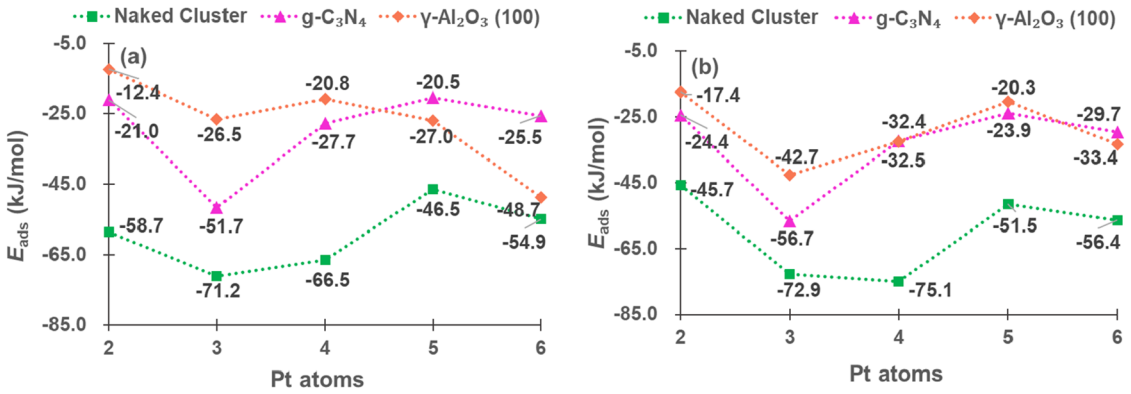

Figure 6. E_{ads} (kJ/mol) of propane, C_1 adsorption (a) and C_2 adsorption (b) on isolated clusters and supported on g-C_3N_4 and γ-Al_2O_3(100).

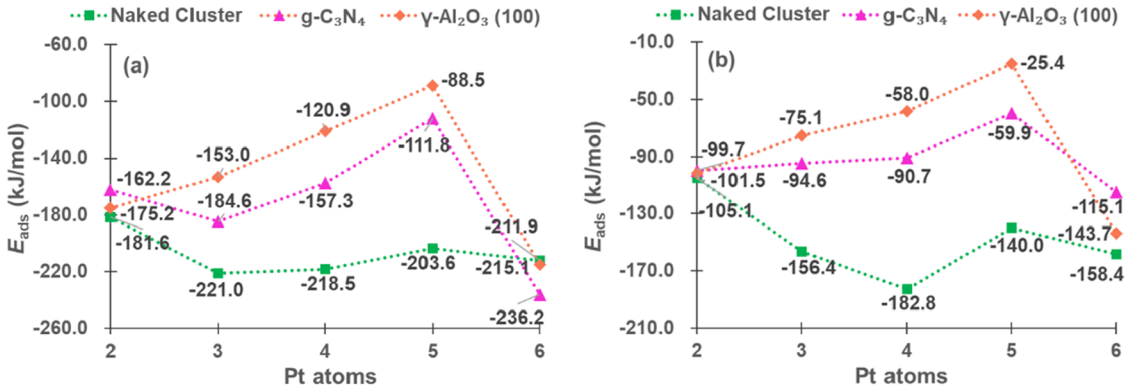

Figure 7. E_{ads} (kJ/mol) of propene (a) and hydrogen (b).

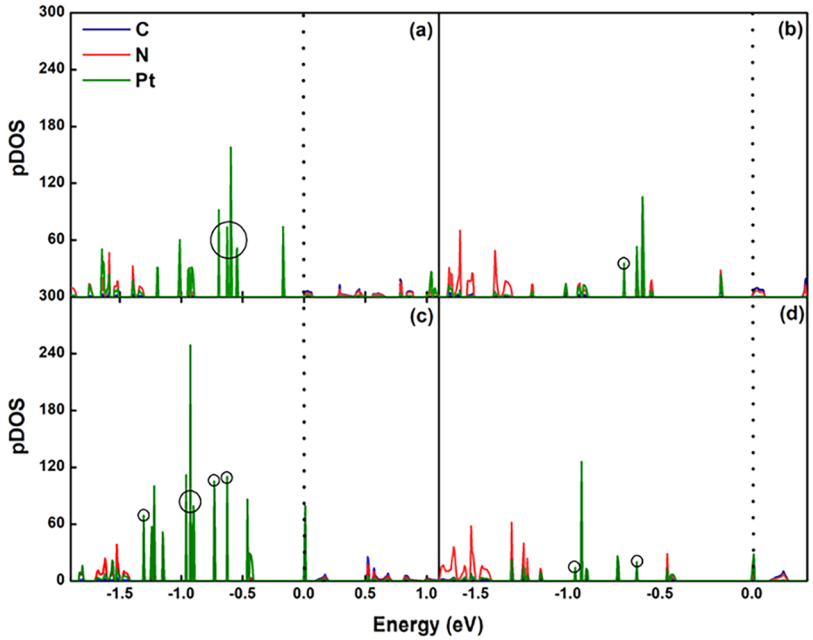

Figure 8. pDOS for Pt_5/g-C_3N_4 (a, b) and Pt_6/g-C_3N_4 (c, d), where (a) and (c) included all C, N, and Pt atoms, and (b) and (d) included all C and N, only the top Pt atom interacting with the molecule. Energy is referred to Fermi energy, and the band gap of g-C_3N_4 is 1.6 eV from our previous study.[29]

(Figure 6a,b, respectively): (1) Propane, as expected, exhibits a weak interaction with E_{ads} ranging from −75.1 to −12.4 kJ/mol for all catalysts; (2) the naked clusters are more active than the supported ones, especially Pt_3 and Pt_4; and (3) the E_{ads} on clusters supported on γ-Al_2O_3(100) and g-C_3N_4 are similar.

We also evaluated the adsorption energies of propene (Figure 7a) and hydrogen (Figure 7b), which are related to the selectivity of PDH. As displayed in Figure 7a, the bare clusters adsorb propene more strongly, particularly Pt_3, Pt_4, and Pt_6, while for Pt_2 and Pt_5, the E_{ads} are lower; the adsorption

https://doi.org/10.1021/acsomega.5c07626
ACS Omega 2025, 10, 46105−46114

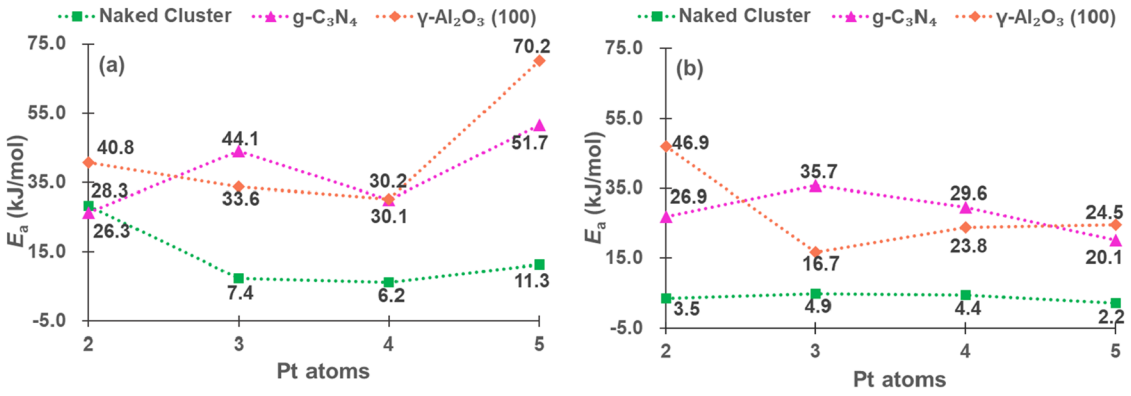

Figure 9. E_a (kJ/mol) for the first (a) and second (b) C−H bond cleavage of propane (C_1 adsorption).

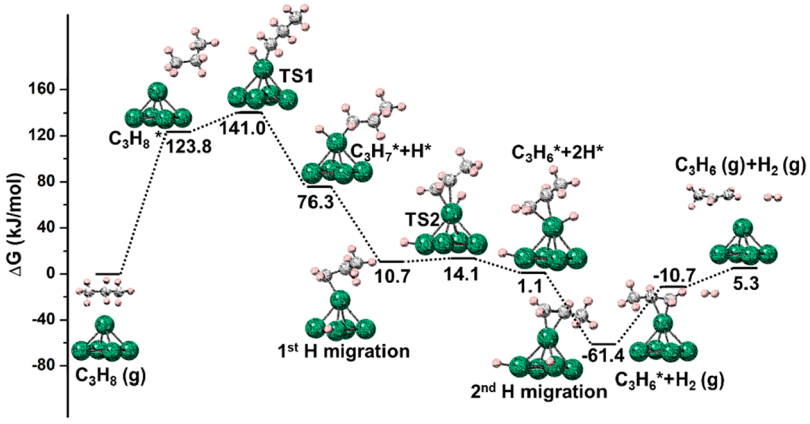

Figure 10. PDH free energy profile on Pt_5 at 873.15 K, for C_1 adsorption. C, H, and Pt atoms are in gray, pink, and green, respectively.

energies on the supported clusters generally weaken as cluster size increases, reaching the weakest point for Pt_5, while they strengthen significantly for Pt_6. Additionally, the E_{ads} of propene is similar on both types of supports, with those on Pt_6 being the stronger ones.

Figure 7b shows that for hydrogen adsorption on naked clusters, the same trend as propene adsorption is observed, E_{ads} is higher on Pt_3, Pt_4 and Pt_6, being lower on Pt_2 and Pt_5; on γ-Al_2O_3(100) and g-C_3N_4, the E_{ads} weakens with cluster size from Pt_2 to Pt_5 but strengthens for Pt_6, and Pt_5 shows relatively low adsorption energy for all the systems.

Previous studies have demonstrated that both geometric and electronic factors affect the catalytic performance of Pt nanoparticles, with electronic factors becoming more dominant when the particles are smaller than 10 nm.[48,49] Thus, the projected densities of states (pDOS in Figure 8) for Pt_5/g-C_3N_4 and Pt_6/g-C_3N_4 were analyzed to investigate the strong adsorption behavior of supported Pt_6 toward propene and hydrogen. As shown in Figure 8, the supported Pt_6 cluster exhibits more unpaired electrons (highlighted by circles) compared to Pt_5, which facilitates molecular adsorption. In Pt_5 (Figure 8b), only one unpaired electron is located on the top Pt atom, leading to weaker adsorption of propene and hydrogen. In contrast, Pt_6 (Figure 8d) features two unpaired electrons on its top Pt atom, which enhances π interactions with propene and promotes chemisorption of hydrogen, thereby resulting in higher adsorption energies. In addition, the supported Pt_6 NPs are expected to exhibit significantly stronger adsorption capability due to an additional exposed Pt atom, consistent with previous findings that the catalytic activity of Pt particles increases with the number of Pt atoms located at faces and corners.[49] Thus, Pt_6 was not further considered in subsequent analyses because of the high adsorption energies of propene and hydrogen, which can reduce the PDH performance.

The performance of clusters (from Pt_2 to Pt_5) was further investigated by the comparison of E_a (Figure 9 for C_1 adsorption and Figure S2 for C_2 adsorption) in the breakage of two C−H bonds of propane. For the first C−H bond breaking, all catalysts show low energy barriers, especially for bare Pt_3 and Pt_4, which are nearly barrierless. In this step, Pt_5 revealed slightly less activity than the others. These findings are similar to the results described by Ge et al.[18] for the C−H activation of propane using a molecular model of Pt_n (n = 2−6) (Figure S3). For the second C−H bond, the scission on all isolated clusters is almost barrier-free (below 5.0 kJ/mol). In the case of g-C_3N_4, the activation energies (Figure 9) first increased with size and then decreased, with the highest barrier for Pt_3/g-C_3N_4. However, on γ-Al_2O_3(100), Pt_3 provided the lowest barrier, which increased gradually with the cluster size.

Based on the information above, as all clusters show high activities toward C−H cleavage, the factors determining the catalytic performance should be the stability and selectivity, with Pt_5 presenting slightly better values.

Free Energy Profiles for PDH on Bare and Supported Pt_5. Herein, the free energy profiles were computed at 873.15 K (C_1 and C_2 adsorption are shown in Figures 10 and S4, respectively). Since the results of C_1 and C_2 are similar, only C_1 adsorption is discussed. As displayed in Figure 10, the calculated adsorption energy of propane was 123.8 kJ/mol,

https://doi.org/10.1021/acsomega.5c07626
ACS Omega 2025, 10, 46105−46114

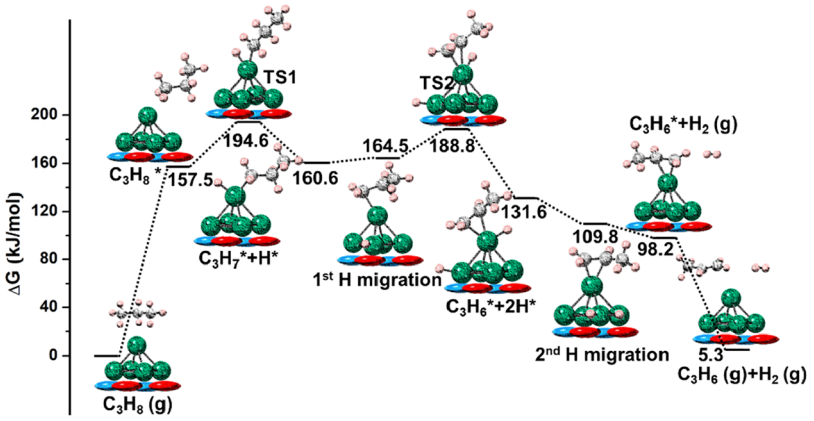

Figure 11. PDH free energy profile on Pt_5/γ-$Al_2O_3(100)$ at 873.15 K, for C_1 adsorption. Color code as in previous figures.

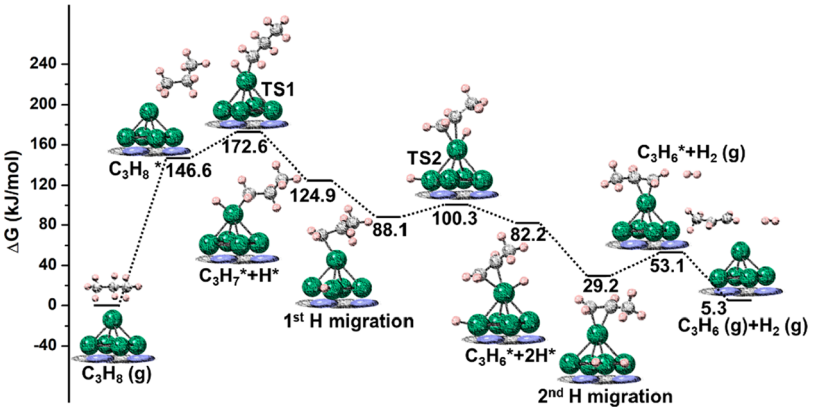

Figure 12. PDH free energy profile on Pt_5/g-C_3N_4 at 873.15 K for C_1 adsorption. Color code as in previous figures.

which can be attributed to the entropic factor. Then, the first C−H bond of propane is activated with a low energy barrier of 17.2 kJ/mol, forming the first intermediate (C_3H_7* + H*), after which the adsorbed hydrogen atom migrates toward another Pt atom, and the hydrogen atom tends to migrate to another Pt atom, leading to a more stable intermediate (1st H migration). Subsequently, the second C−H bond is activated by the same Pt atom with an extremely low barrier of 3.4 kJ/mol, leading to π-adsorbed propene (C_3H_6* + 2H*). Then, the adsorbed hydrogen atom moves to another Pt atom (2nd H migration); the E_{ads} values for different configurations are shown in Table S2. H_2 and propene desorb with 50.7 and 16 kJ/mol, respectively. Thus, the rate-determining step (RDS) of this process should be the desorption, which requires a total energy of 66.7 kJ/mol at 873.15 K. This can be attributed to the strong interactions between the highly active clusters and the adsorbates, highlighting the importance of supports for catalyst modification.

Then, the energy profiles of Pt_5/γ-$Al_2O_3(100)$ under the same conditions as Pt_5 are given in Figure 11 (C_1) and Figure S5 (C_2). The adsorption energy of propane (157.5 kJ/mol) is 33.7 kJ/mol less favorable than for the naked Pt_5 cluster, due to the reduced activity of supported clusters (Figures 6 and 9). Thus, the E_a (37.1 kJ/mol) for the first C−H bond activation is higher (by 17.2 kJ/mol) than for the naked Pt_5 cluster, showing a lower activity for the C−H cleavage. The intermediate after hydrogen migration (1st H migration) is slightly less stable (by 3.9 kJ/mol) than C_3H_7* + H*. However, we assume that the migration occurs to regenerate the top Pt atom and activate the second C−H bond, which is consistent with a previous study on Pt_4-catalyzed PDH.[50] Again, the E_a (24.3 kJ/mol) for the second bond breaking is higher (by 20.9 kJ/mol) than that of the naked cluster, showing a reduced activity. On the positive side, due to the reduced adsorption energies on Pt_5/γ-$Al_2O_3(100)$, the desorption of hydrogen and propene is exergonic at 873.15 K, releasing 11.6 and 92.9 kJ/mol, respectively, and indicating an enhanced selectivity on the γ-$Al_2O_3(100)$ support. Throughout the energy profile, the C−H bond cleavage (TS1) is the RDS for Pt_5/γ-$Al_2O_3(100)$.

Finally, the energy profile of Pt_5/g-C_3N_4 under the same conditions is displayed in Figure 12 (C_1) and Figure S6 (C_2). The adsorption energy of propane is 146.6 kJ/mol, similar to that on Pt_5/γ-$Al_2O_3(100)$ (157.5 kJ/mol) and only slightly higher than on the naked Pt_5 cluster (123.8 kJ/mol). The E_a of the first and second bond breaking are 26.0 and 12.2 kJ/mol, respectively, also falling between Pt_5 (17.2 and 3.4 kJ/mol) and Pt_5/γ-$Al_2O_3(100)$ (37.1 and 24.3 kJ/mol). In addition, the desorption of H_2 and propene for Pt_5/g-C_3N_4 also falls between Pt_5 and Pt_5/γ-$Al_2O_3(100)$. On the one hand, H_2 desorption of Pt_5/g-C_3N_4 is endergonic, but less energy (23.9 kJ/mol) is required, compared to that of naked Pt_5 (50.7 kJ/mol). On the other hand, propene desorption of Pt_5/g-C_3N_4 is exergonic, but less energy (47.8 kJ/mol) is released than on Pt_5/γ-$Al_2O_3(100)$ (92.9 kJ/mol). Catalyst activity and selectivity tend to go in opposite directions. Therefore, it is important that both are balanced. Thus, g-C_3N_4 may be a

https://doi.org/10.1021/acsomega.5c07626
ACS Omega 2025, 10, 46105−46114

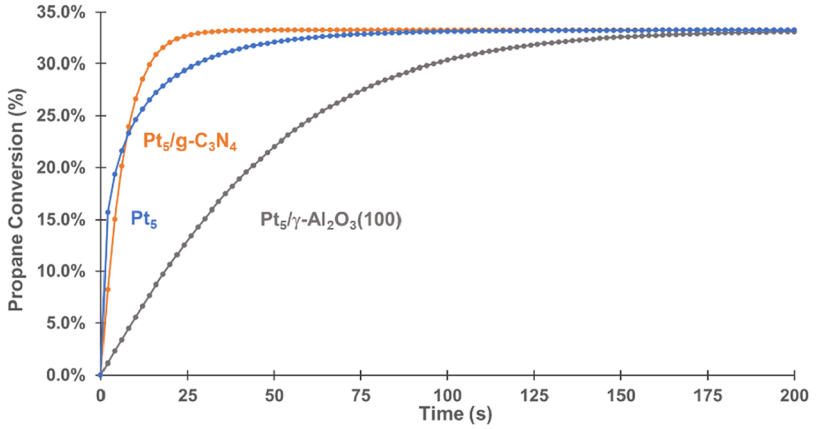

Figure 13. Predicted propane conversion on Pt_5, $Pt_5/g\text{-}C_3N_4$, and $Pt_5/\gamma\text{-}Al_2O_3(100)$ at 873.15 K, 1 atm.

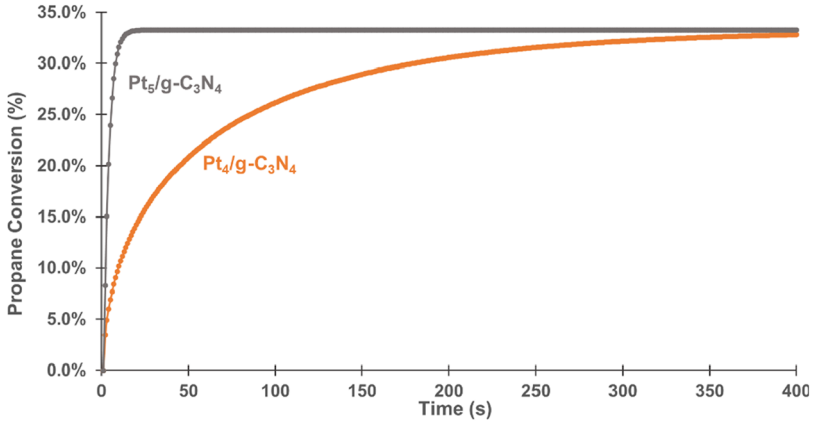

Figure 14. Predicted propane conversion on $Pt_4/g\text{-}C_3N_4$ and $Pt_5/g\text{-}C_3N_4$, at 873.15 K, 1 atm.

better support, as it improves the selectivity while balancing the activity.

Microkinetic Analysis of PDH on Naked and Supported Pt_5. All of the previously considered reactions, as well as the elementary steps for C−C bond breaking of propane, C═C bond breaking of propene, and deep dehydrogenation (Table S3), were included in the microkinetic analysis. All catalysts reached equilibrium conversion at 873.15 K, ca. 33%, which is consistent with our previous results on Pt_1 and $Pt_4/g\text{-}C_3N_4$.[29] In addition, the isolated Pt_5 cluster has the highest activity at initial times (Figure 13) and then is overtaken by $Pt_5/g\text{-}C_3N_4$. This is because of the high coverage of C_3H_6* + 2H* intermediates (about 97%) and C_3H_6* (about 0.8%) on the active site of Pt_5, which corresponds to the cost of desorption (Figure 10). The coverage of C_3H_6* + 2H* on $Pt_5/g\text{-}C_3N_4$ is about 22%, and no other intermediates are detected, which is consistent with the easier H_2 desorption (Figure 12). The lower activity of $Pt_5/\gamma\text{-}Al_2O_3(100)$ is caused by the higher activation energy of TS1 and TS2 (Figure 11). Combined with the Gibbs free energy profiles, microkinetic analysis further confirms the best performance of $Pt_5/g\text{-}C_3N_4$ among the three catalysts.

We have also considered various temperatures around 873.15 K to estimate an apparent activation energy at initial times for the reaction following the Arrhenius equation. The results satisfied the linearity of the Arrhenius plot. The apparent activation energies were found to be 27, 40, and 49 kJ/mol for Pt_5, $Pt_5/g\text{-}C_3N_4$, and $Pt_5/\gamma\text{-}Al_2O_3(100)$, respectively. This is in agreement with the apparent activation energy of $Pt_4/g\text{-}C_3N_4$ (57 kJ/mol), previously studied in our group.[29] These estimations are also similar to the values obtained by Sui and Chen et al. for PDH on Pt/Al_2O_3 nanocatalysts, obtaining a value of 41 ± 5 kJ/mol for subnanometric clusters.[21]

In addition, the performance of $Pt_5/g\text{-}C_3N_4$ was also compared with $Pt_4/g\text{-}C_3N_4$.[29] We found that $Pt_5/g\text{-}C_3N_4$ was slightly more active than $Pt_4/g\text{-}C_3N_4$ (Figure 14), according to the Gibbs free energy profiles (Figure S7).

The profiles indicate that the free energy barriers for both $Pt_4/g\text{-}C_3N_4$ and $Pt_5/g\text{-}C_3N_4$ are similar, suggesting comparable activity for the C−H cleavage of propane. However, the desorption of H_2 on Pt_4 is more costly, due to the formation of a relatively deep energy well in C_3H_6* + H* + H* (2nd H migration step). In contrast, on Pt_5, the desorption process is favored, leading to a better PDH performance.

CONCLUSIONS

The performance of small Pt clusters, ranging from Pt_2 to Pt_6, as catalysts for PDH was investigated by means of theoretical calculations and compared with that supported on $\gamma\text{-}Al_2O_3(100)$ and $g\text{-}C_3N_4$. The study reveals that both cohesion and interaction energies become stronger as the Pt cluster size increases, with the most stable surface−cluster interaction corresponding to adsorbed Pt_5. The adsorption energies of propane on Pt_n, $Pt_n/\gamma\text{-}Al_2O_3(100)$, and $Pt_n/g\text{-}C_3N_4$ are comparable, resulting in similar energy barriers for the first and the second C−H bond breaking of propane (all barriers are lower than 47 kJ/mol). For the supported clusters, the

https://doi.org/10.1021/acsomega.5c07626
ACS Omega 2025, 10, 46105−46114

adsorption energy of propene and hydrogen weakens when increasing the size of the Pt clusters until Pt_5. At 873.15 K for Pt_5, both desorption of hydrogen and propene are endergonic; while for Pt_5/γ-$Al_2O_3(100)$, both desorption processes are exergonic; and for Pt_5/g-C_3N_4, the desorption of hydrogen is endergonic while the desorption of propene is exergonic.

Among the analyzed systems, both naked and supported Pt_5 particles show the best performance in PDH in terms of stability, activity, and desorption. Moreover, the comparison of naked and supported Pt_5 clusters reveals that the support is essential to tune the stability and desorption capacity of the catalysts. On Pt_5/γ-$Al_2O_3(100)$, desorption is easier (for both H_2 and propene) than on Pt_5/g-C_3N_4; however, the activation of propane follows the opposite trend, leading to the better PDH performance of Pt_5/g-C_3N_4. Moreover, the performance of Pt_5/g-C_3N_4 is also better than that of the previously studied Pt_4/g-C_3N_4. The microkinetic analysis shows that deep dehydrogenation and C−C bond cleavage are rare events within the studied clusters, indicating a high selectivity for all of them.

■ ASSOCIATED CONTENT

Data Availability Statement

All of the structures can be retrieved from the ioChem-BD database.[51] (DOI: 10.19061/iochem-bd-2-83).

Supporting Information

The Supporting Information is available free of charge at https://pubs.acs.org/doi/10.1021/acsomega.5c07626.

The thermodynamic calculations, additional tables, and figures for the relevant structures and the C_2 pathways. (PDF)

■ AUTHOR INFORMATION

Corresponding Author

Josep M. Ricart − *Departament de Química Física i Inorgànica, Universitat Rovira i Virgili, 43007 Tarragona, Spain;* orcid.org/0000-0002-2610-5535; Email: josep.ricart@urv.cat

Authors

Jie Pan − *Departament de Química Física i Inorgànica, Universitat Rovira i Virgili, 43007 Tarragona, Spain*

Gerard Bru − *Departament de Química Física i Inorgànica, Universitat Rovira i Virgili, 43007 Tarragona, Spain*

Jorge J. Carbó − *Departament de Química Física i Inorgànica, Universitat Rovira i Virgili, 43007 Tarragona, Spain;* orcid.org/0000-0002-3945-6721

Cyril Godard − *Departament de Química Física i Inorgànica, Universitat Rovira i Virgili, 43007 Tarragona, Spain;* orcid.org/0000-0001-5762-4904

Complete contact information is available at: https://pubs.acs.org/10.1021/acsomega.5c07626

Author Contributions

The manuscript was written through the contributions of all authors. All authors have given approval to the final version of the manuscript.

Notes

The authors declare no competing financial interest.

■ ACKNOWLEDGMENTS

This work was supported (PID2021-128128NB-I00 and PID2019-104427RB-I00) by "MICIU/AEI/10.13039/501100011033 and "FEDER/UE" and (2021SGR00110 and 2021SGR00163) by Generalitat de Catalunya. J.P. thanks AGAUR from the Generalitat de Catalunya for the grant 2020-FISDU-00174.

■ REFERENCES

(1) Cognitive Market Research. Polypropylene Glycol Market Report 2024 2024 https://www.cognitivemarketresearch.com/polypropylene-glycol-market-report (accessed April 16, 2025).

(2) Chen, S.; Chang, X.; Sun, G.; Zhang, T.; Xu, Y.; Wang, Y.; Pei, C.; Gong, J. Propane dehydrogenation: catalyst development, new chemistry, and emerging technologies. *Chem. Soc. Rev.* **2021**, *50*, 3315−3354.

(3) Zhong, J.; Han, J.; Wei, Y.; Liu, Z.; et al. Recent Advances of the Nano-Hierarchical SAPO-34 in the Methanol-to-Olefin (MTO) Reaction and Other Applications. *Catal. Sci. Technol.* **2017**, *7*, 4905−4923.

(4) Yarulina, I.; De Wispelaere, K.; Bailleul, S.; Goetze, J.; Radersma, M.; Abou-Hamad, E.; Hazemann, J.-L.; Olsbye, U.; Weckhuysen, B. M.; Van Speybroeck, V.; Kapteijn, F.; Gascon, J.; et al. Structure−Performance Descriptors and the Role of Lewis Acidity in the Methanol-to-Propylene Process. *Nat. Chem.* **2018**, *10*, 804−812.

(5) Munnik, P.; De Jongh, P. E.; De Jong, K. P. Control and Impact of the Nanoscale Distribution of Supported Cobalt Particles Used in Fischer−Tropsch Catalysis. *J. Am. Chem. Soc.* **2014**, *136*, 7333−7340.

(6) van de Loosdrecht, J.; Van De Loosdrecht, J.; Ciobîca, I. M.; Gibson, P.; Govender, N. S.; Neuenschwander, U.; Moodley, D. J.; Van Berge, P.; Saib, A. M.; Oukaci, R.; Weststrate, C. J.; Visagie, J. L. Providing Fundamental and Applied Insights into Fischer−Tropsch Catalysis: Sasol−Eindhoven University of Technology Collaboration. *ACS Catal.* **2016**, *6*, 3840−3855.

(7) Sattler, J. J. H. B.; Ruiz-Martinez, J.; Santillan-Jimenez, E.; Weckhuysen, B. M. Catalytic Dehydrogenation of Light Alkanes on Metals and Metal Oxides. *Chem. Rev.* **2014**, *114*, 10613−10653.

(8) Nawaz, Z. Light Alkane Dehydrogenation to Light Olefin Technologies: A Comprehensive Review. *Rev. Chem. Eng.* **2015**, *31*, 413−436.

(9) Saudi Basic Industries Corp. Alkane Dehydrogenation Catalyst and Process for Its Preparation. WIPO Patent WO2014016810A1, 2014.

(10) Wang, G.; Zhu, X.; Li, C. Recent Progress in Commercial and Novel Catalysts for Catalytic Dehydrogenation of Light Alkanes. *Chem. Rec.* **2020**, *20*, 604−616.

(11) Xiao, L.; Ma, F.; Zhu, Y. A.; Sui, Z. J.; Zhou, J. H.; Zhou, X. G.; Chen, D.; Yuan, W. K. Improved Selectivity and Coke Resistance of Core−Shell Alloy Catalysts for Propane Dehydrogenation from First Principles and Microkinetic Analysis. *Chem. Eng. J.* **2019**, *377*, 120049−120059.

(12) Sun, X.; Liu, M.; Huang, Y.; Li, B.; Zhao, Z. Electronic Interaction Between Single Pt atom and Vacancies on Boron Nitride Nanosheets and its Influence on the Catalytic Performance in the Direct Dehydrogenation of Propane. *Chin. J. Catal.* **2019**, *40*, 819−825.

(13) Nijhuis, T. A. X.; Tinnemans, S. J.; Visser, T.; Weckhuysen, B. M. Operando Spectroscopic Investigation of Supported Metal Oxide Catalysts by Combined Time-Resolved UV-Vis/Raman/On-Line Mass Spectrometry. *Phys. Chem. Chem. Phys.* **2003**, *5*, 4361−4365.

(14) Yang, M.-L.; Zhu, J.; Zhu, Y. - A.; Sui, Z. - J.; Yu, Y. - D.; Zhou, X.- G.; Chen, D. Tuning Selectivity and Stability in Propane Dehydrogenation by Shaping Pt Particles: A Combined Experimental and DFT Study. *J. Mol. Catal. A* **2014**, *395*, 329−336.

(15) Zhu, Y.; An, Z.; Song, H.; Xiang, X.; Yan, W.; He, J. Lattice-Confined Sn (IV/II) Stabilizing Raft-Like Pt Clusters: High Selectivity and Durability in Propane Dehydrogenation. *ACS Catal.* **2017**, *7*, 6973−6978.

(16) Liu, J.; Yue, Y.; Liu, H.; Da, Z.; Liu, C.; Ma, A.; Rong, J.; Su, D.; Bao, X.; Zheng, H. Origin of the Robust Catalytic Performance ofNanodiamond− Graphene-Supported Pt Nanoparticles Used in the Propane Dehydrogenation Reaction. *ACS Catal.* **2017**, *7*, 3349−3355.
(17) Zhu, J.; Yang, M. L.; Yu, Y.; Zhu, Y. A.; Sui, Z. J.; Zhou, X. G.; Holmen, A.; Chen, D. Size-Dependent Reaction Mechanism and Kinetics for Propane Dehydrogenation over Pt Catalysts. *ACS Catal.* **2015**, *5*, 6310−6319.
(18) Shore, T. C.; Mith, D.; Deprekel, D.; McNall, S.; Ge, Y. A B3LYP study on the C−H activation in propane by neutral and +1 charged low-energy platinum clusters with 2−6 atoms. *React. Kinet. Mech. Catal.* **2013**, *109*, 315−333.
(19) Vajda, S.; Pellin, M. J.; Greeley, J. P.; Marshall, C. L.; Curtiss, L. A.; Ballentine, G. A.; Elam, J. W.; Catillon-Mucherie, S.; Redfern, P. C.; Mehmood, F.; Zapol, P. Subnanometre platinum clusters as highly active and selective catalysts for the oxidative dehydrogenation of propane. *Nat. Mater.* **2009**, *8*, 213−216.
(20) Hu, C. H.; Chizallet, C.; Mager-Maury, C.; Corral-Valero, M.; Roudier, S.; Sautet, P.; Sastre, G.; Toulhoat, H.; Visse, F. Modulation of Catalyst Particle Structure upon Support Hydroxylation: Ab Initio Insights into Pd_{13} and Pt_{13}/γ-Al_2O_3. *J. Catal.* **2010**, *274*, 99−110.
(21) Zhang, W.; Wang, H.; Jiang, J.; Sui, Z.; Zhu, Y.; Chen, D.; Zhou, X. Size Dependence of Pt Catalysts for Propane Dehydrogenation: from Atomically Dispersed to Nanoparticles. *ACS Catal.* **2020**, *10*, 12932−12942.
(22) Gorczyca, A.; Raybaud, P.; Moizan, V.; Joly, Y.; Chizallet, C. Atomistic Models for Highly-Dispersed PtSn/γ-Al_2O_3 Catalysts: Ductility and Dilution Affect the Affinity for Hydrogen. *ChemCatChem* **2019**, *11*, 3941−3951.
(23) Mei, D.; Kwak, J. H.; Hu, J.; Cho, S. J.; Szanyi, J.; Allard, L. F.; Peden, C. H. F. Unique Role of Anchoring Penta-Coordinated Al^{3+} Sites in the Sintering of γ-Al_2O_3-Supported Pt Catalysts. *J. Phys. Chem. Lett.* **2010**, *1*, 2688−2691.
(24) Chen, Z.; Zhao, J.; Cabrera, C. R.; Chen, Z. Computational Screening of Efficient Single-Atom Catalysts Based on Graphitic Carbon Nitride (g-C_3N_4) for Nitrogen Electroreduction. *Small Methods* **2019**, *3*, 1800368−1800377.
(25) Vorobyeva, E.; Fako, E.; Chen, Z.; Collins, S. M.; Johnstone, D.; Midgley, P. A.; Hauert, R.; Safonova, O. V.; Vilé, G.; López, N.; Mitchell, S.; Pérez-Ramírez, J. Atom-by-Atom Resolution of Structure-Function Relations over Low-Nuclearity Metal Catalysts. *Angew. Chem.* **2019**, *131*, 8816−8821.
(26) Kong, N.; Fan, X.; Liu, F.; Wang, L.; Lin, H.; Li, Y.; Lee, S. T. Single Vanadium Atoms Anchored on Graphitic Carbon Nitride as a High Performance Catalyst for Non-oxidative Propane Dehydrogenation. *ACS Nano* **2020**, *14*, 5772−5779.
(27) Pan, J.; Plana-Ruiz, S.; Taoufik, M.; Curulla-Ferré, D.; Godard, C.; Ricart, J. M. Switchable selectivity in styrene hydroformylation using single-atom Rh/g-C_3N_4 catalysts. *ACS Appl. Nano Mater.* **2025**, *8* (13), 6737−6746.
(28) Salom-Català, A.; Strugovshchikov, E.; Kaźmierczak, K.; Curulla-Ferré, D.; Ricart, J. M.; Carbó, J. J. Reactive Force Field Development for Propane Dehydrogenation on Platinum Surfaces. *J. Phys. Chem. C* **2024**, *128*, 2844−2855.
(29) Pan, J.; Strugovshchikov, E.; Salóm-Català, A.; Novell-Leruth, G.; Kaźmierczak, K.; Curulla-Ferré, D.; Carbó, J. J.; Godard, C.; Ricart, J. M. Propane Dehydrogenation on Pt Single-Atom and Pt_4 and Pt_3Sn Single-Cluster Supported on g-C_3N_4: A Theoretical Study. *J. Phys. Chem. C* **2025**, *129*, 2477−2487.
(30) Kresse, G.; Furthmüller, J. Efficient iterative Schemes for Ab initio Total-energy Calculations Using a Plane-wave Basis Set. *Phys. Rev. B* **1996**, *54*, 11169−11186.
(31) Blöchl, P. E. Projector Augmented-wave Method. *Phys. Rev. B* **1994**, *50*, 17953−17979.
(32) Perdew, J. P.; Burke, K.; Ernzerhof, M. Generalized Gradient Approximation Made Simple. *Phys. Rev. Lett.* **1996**, *77*, 3865−3868.
(33) Grimme, S.; Antony, J.; Ehrlich, S.; Krieg, H. A Consistent and Accurate Ab Initio Parametrization of Density Functional Dispersion Correction (DFT-D) for the 94 elements H-Pu. *J. Chem. Phys.* **2010**, *132*, 154104−154124.
(34) Bader, R. F. W. *Atoms in Molecules: A Quantum Theory*; Oxford University Press: Oxford, U.K., 1990.
(35) Chaves, A. S.; Piotrowski, M. J.; Da Silva, J. L. F. Evolution of the structural, energetic, and electronic properties of the 3d, 4d, and 5d transition-metal clusters (30 TMn systems for n = 2-15): a density functional theory investigation. *Phys. Chem. Chem. Phys.* **2017**, *19*, 15484−15502.
(36) Wang, Y.; Xiang, B.; Yang, H. Q.; Hu, C. W. A. Density Functional Theory Study on the Nucleation and Growth of Ptn Clusters on γ-Al_2O_3(001) Surface. *ACS Omega* **2017**, *2*, 3250−3259.
(37) Jennings, P. C.; Johnston, R. L. Structures of small Ti- and V-doped Pt clusters: A GA-DFT study. *Comput. Theor. Chem.* **2013**, *1021*, 91−100.
(38) Maldonado, A. S.; Cabeza, G. F.; Ramos, S. B. Dynamical stability and vibrational properties of Pt clusters. *J. Phys. Chem. Solids* **2019**, *131*, 131−138.
(39) Mager-Maury, C.; Chizallet, C.; Sautet, P.; Raybaud, P. Platinum Nanoclusters Stabilized on γ-Alumina by Chlorine Used As a Capping Surface Ligand: A Density Functional Theory Study. *ACS Catal.* **2012**, *2*, 1346−1357.
(40) Mager-Maury, C.; Bonnard, G.; Chizallet, C.; Sautet, P.; Raybaud, P. H_2-Induced Reconstruction of Supported Pt Clusters: Metal−Support Interaction versus Surface Hydride. *ChemCatChem* **2011**, *3*, 200−207.
(41) Digne, M.; Sautet, P.; Raybaud, P.; Euzen, P.; Toulhoat, H. A. Hydroxyl Groups on γ-Alumina Surfaces: A DFT Study. *J. Catal.* **2002**, *211*, 1−5.
(42) Digne, M.; Sautet, P.; Raybaud, P.; Euzen, P.; Toulhoat, H. A. Use of DFT to achieve a rational understanding of acid−basic properties of γ-alumina surfaces. *J. Catal.* **2004**, *226*, 54−68.
(43) Hu, C. H.; Chizallet, C.; Mager-Maury, C.; Corral-Valero, M.; Sautet, P.; Toulhoat, H.; Raybaud, P. Modulation of Catalyst Particle Structure upon Support Hydroxylation: Ab Initio Insights into Pd_{13} and Pt_{13}/γ-Al_2O_3. *J. Catal.* **2010**, *274*, 99−110.
(44) Nigam, S.; Majumder, C. ORR viability of alumina-supported platinum nanocluster: exploring oxidation behaviour by DFT. *Phys. Chem. Chem. Phys.* **2017**, *19*, 19308−19315.
(45) Cai, J.; Wei, L.; Liu, J.; Xue, C.; Chen, Z.; Hu, Z.; Zang, Y.; Wang, M.; Shi, W.; Qin, T.; Zhang, H.; Chen, L.; Liu, X.; Willinger, M. G.; Hu, P.; Liu, K.; Yang, B.; Liu, Z.; Liu, Z.; Wang, Z. J. Two-dimensional crystalline platinum oxide. *Nat. Mater.* **2024**, *23*, 1654−1663.
(46) Huang, X.; Xia, Y.; Cao, Y.; Zheng, X.; Pan, H.; Zhu, J.; Ma, C.; Wang, H.; Li, J.; You, R.; Wei, S.; Huang, W.; Lu, J. Enhancing both selectivity and coking-resistance of a single-atom Pd_1/C_3N_4 catalyst for acetylene hydrogenation. *Nano Res.* **2017**, *10*, 1302−1312.
(47) Chen, Z.; Mitchell, S.; Vorobyeva, E.; Leary, R. K.; Hauert, R.; Furnival, T.; Ramasse, Q. M.; Thomas, J. M.; Midgley, P. A.; Dontsova, D.; Antonietti, M.; Pogodin, S.; López, N.; Pérez-Ramírez, J. Stabilization of Single Metal Atoms on Graphitic Carbon Nitride. *Adv. Funct. Mater.* **2017**, *27*, 1605785−1605797.
(48) Chen, T.; Ye, L.; Lo, T. W. B. Designing the electronic and geometric structures of single-atom and nanocluster catalysts. *J. Mater. Chem. A* **2021**, *9*, 18773−18784.
(49) Strizhak, P. E.; Trypolskyi, A. I.; Kosmambetova, G. R.; Didenko, O. Z.; Gurnyk, T. N. Geometric and electronic approaches to size effects in heterogeneous catalysis. *Kinet. Catal* **2011**, *52*, 128−138.
(50) Hauser, A. W.; Gomes, J.; Bajdich, M.; Head-Gordon, M.; Bell, A. T. Subnanometer-sized Pt/Sn Alloy Cluster Catalysts for the Dehydrogenation of Linear Alkanes. *Phys. Chem. Chem. Phys.* **2013**, *15*, 20727−207285.
(51) Álvarez-Moreno, M.; de Graaf, C.; López, N.; Maseras, F.; Poblet, J. M.; Bo, C. Managing the Computational Chemistry Big Data Problem: The ioChem-BD Platform. *J. Chem. Inf. Model.* **2015**, *55*, 95−103.

https://doi.org/10.1021/acsomega.5c07626
ACS Omega 2025, 10, 46105−46114